RESEARCH ARTICLE | JANUARY 03 2023

Readout of a quantum processor with high dynamic range Josephson parametric amplifiers **⊙**⊘

Theodore White \blacksquare 0; Alex Opremcak; George Sterling 0; Alexander Korotkov; Daniel Sank 0; Rajeev Acharya; Markus Ansmann (1); Frank Arute (1); Kunal Arya (1); Joseph C. Bardin; Andreas Bengtsson [0]; Alexandre Bourassa [0]; Jenna Bovaird [0]; Leon Brill; Bob B. Buckley; David A. Buell; Tim Burger 🗓 ; Brian Burkett 🗓 ; Nicholas Bushnell; Zijun Chen; Ben Chiaro; Josh Cogan; Roberto Collins; Alexander L. Crook [0]; Ben Curtin [0]; Sean Demura; Andrew Dunsworth [0]; Catherine Erickson [0]; Reza Fatemi 💿 ; Leslie Flores Burgos; Ebrahim Forati; Brooks Foxen 👨 ; William Giang; Marissa Giustina 👨 ; Alejandro Grajales Dau 📵 ; Michael C. Hamilton 📵 ; Sean D. Harrington 📵 ; Jeremy Hilton; Markus Hoffmann [®]; Sabrina Hong; Trent Huang; Ashley Huff; Justin Iveland [®]; Evan Jeffrey [®]; Mária Kieferová 👵 ; Seon Kim 👵 ; Paul V. Klimov 💿 ; Fedor Kostritsa; John Mark Kreikebaum 👵 ; David Landhuis [0]; Pavel Laptev; Lily Laws; Kenny Lee; Brian J. Lester [0]; Alexander Lill [0]; Wayne Liu; Aditya Locharla; Erik Lucero 📵 ; Trevor McCourt 📵 ; Matt McEwen 📵 ; Xiao Mi 📵 ; Kevin C. Miao 📵 ; Shirin Montazeri 🗓 ; Alexis Morvan 🗓 ; Matthew Neeley 🗓 ; Charles Neill; Ani Nersisyan 🗓 ; Jiun How Ng; Anthony Nguyen [0]; Murray Nguyen; Rebecca Potter; Chris Quintana; Pedram Roushan [0]; Kannan Sankaragomathi 📵 ; Kevin J. Satzinger 📵 ; Christopher Schuster; Michael J. Shearn 📵 ; Aaron Shorter; Vladimir Shvarts; Jindra Skruzny; W. Clarke Smith [6]; Marco Szalay; Alfredo Torres; Bryan W. K. Woo [6]; Z. Jamie Yao; Ping Yeh; Juhwan Yoo; Grayson Young; Ningfeng Zhu 💿; Nicholas Zobrist 💿; Yu Chen; Anthony Megrant; Julian Kelly; Ofer Naaman

©

Check for updates

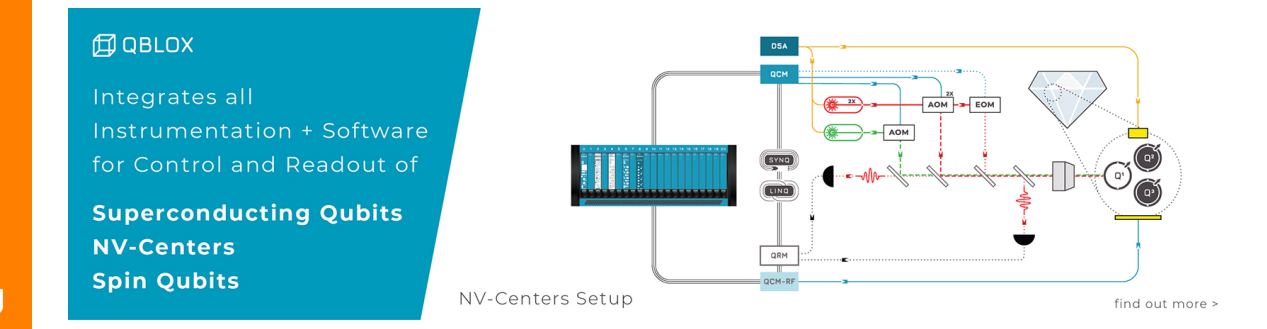
Appl. Phys. Lett. 122, 014001 (2023) https://doi.org/10.1063/5.0127375





CrossMark

Export Citation





Readout of a quantum processor with high dynamic range Josephson parametric amplifiers ()

Cite as: Appl. Phys. Lett. **122**, 014001 (2023); doi: 10.1063/5.0127375 Submitted: 21 September 2022 · Accepted: 21 November 2022 · Published Online: 3 January 2023







Theodore White, ^{1,a)} D Alex Opremcak, George Sterling, Dalexander Korotkov, Daniel Sank, Dan
Brian Burkett, Dicholas Bushnell, Zijun Chen, Ben Chiaro, Josh Cogan, Roberto Collins, Alexander L. Crook,
D Ben Curtin, D Sean Demura, Andrew Dunsworth, D Catherine Erickson, D Reza Fatemi, D
Leslie Flores Burgos, Ebrahim Forati, Brooks Foxen, DWilliam Giang, Marissa Giustina, D
Alejandro Grajales Dau, 1 (b) Michael C. Hamilton, 13 (b) Sean D. Harrington, 1 (b) Jeremy Hilton, 1 Markus Hoffmann, 1 (b)
Sabrina Hong, Trent Huang, Ashley Huff, Justin Iveland, 6 Evan Jeffrey, 6 Mária Kieferová, 6 Seon Kim, 6
Paul V. Klimov, no Fedor Kostritsa, John Mark Kreikebaum, no David Landhuis, no Pavel Laptev, Lily Laws,
Kenny Lee, Brian J. Lester, 6 Alexander Lill, 6 Wayne Liu, Aditya Locharla, Erik Lucero, 6 Trevor McCourt, 6
Matt McEwen, 14 (b) Xiao Mi, 16 Kevin C. Miao, 16 Shirin Montazeri, 16 Alexis Morvan, 16 Matthew Neeley, 16
Charles Neill, Ani Nersisyan, Diun How Ng, Anthony Nguyen, DMurray Nguyen, Rebecca Potter,
Chris Quintana, Pedram Roushan, 🕞 Kannan Sankaragomathi, 🕞 Kevin J. Satzinger, 🕞 Christopher Schuster,
Michael J. Shearn, 🔞 Aaron Shorter, Vladimir Shvarts, Jindra Skruzny, W. Clarke Smith, 📵 Marco Szalay,
Alfredo Torres, Bryan W. K. Woo, D. Z. Jamie Yao, Ping Yeh, Juhwan Yoo, Grayson Young, Ningfeng Zhu,
Nicholas Zobrist, 1 D Yu Chen, 1 Anthony Megrant, 1 Julian Kelly, 1 and Ofer Naaman 1.a) D

AFFILIATIONS

ABSTRACT

We demonstrate a high dynamic range Josephson parametric amplifier (JPA) in which the active nonlinear element is implemented using an array of rf-SQUIDs. The device is matched to the $50~\Omega$ environment with a Klopfenstein-taper impedance transformer and achieves a bandwidth of 250-300~MHz with input saturation powers up to -95~dBm at 20~dB gain. A 54-qubit Sycamore processor was used to benchmark these devices, providing a calibration for readout power, an estimation of amplifier added noise, and a platform for comparison against standard impedance matched parametric amplifiers with a single dc-SQUID. We find that the high power rf-SQUID array design has no adverse effect on system noise, readout fidelity, or qubit dephasing, and we estimate an upper bound on amplifier added noise at 1.6 times the quantum limit. Finally, amplifiers with this design show no degradation in readout fidelity due to gain compression, which can occur in multitone multiplexed readout with traditional JPAs.

Published under an exclusive license by AIP Publishing. https://doi.org/10.1063/5.0127375

Dispersive readout¹ of superconducting qubits requires the use of near quantum limited superconducting amplifiers because of the severe limits placed by the quantum system on the allowed microwave probe power.² Resonant Josephson parametric amplifiers (JPAs) have been popular in single qubit readout as they provide high gain, quantum-limited noise performance, tunable center frequency,³⁻⁶

and are simple to manufacture. However, larger quantum processors typically multiplex qubit measurement in the frequency domain, transmitting and receiving multiple probe tones using the same readout line. This configuration requires a first stage amplifier with higher bandwidth and saturation power than the typical JPAs can provide.

¹Google Quantum Al, Goleta, California 93117, USA

²Department of Electrical and Computer Engineering, University of Massachusetts, Amherst Massachusetts 01003, USA

³Department of Electrical and Computer Engineering, Auburn University, Auburn, Alabama 36849, USA

⁴Department of Physics, University of California, Santa Barbara, California 93106, USA

^{a)}Authors to whom correspondence should be addressed: tcwhite@google.com and ofernaaman@google.com

The instantaneous bandwidth of resonant JPAs can be increased using impedance matching techniques, 8-11 but their input saturation power remains low, -115 to -110 dBm. High dynamic range JPAs using SQUID arrays have been demonstrated, 12,13 but while improving the input saturation power up to -95 dBm, they still suffer from relatively narrow bandwidths, less than 200 MHz. Traveling wave parametric amplifiers (TWPAs) can provide bandwidths in excess of 2 GHz and high saturation power 14-18 but are difficult to fabricate and typically have lower quantum efficiency than JPAs due to higher dissipative and intermodulation losses. 19 Practical systems' considerations, such as qubit frequency placement plan, 20 Purcell filter bandwidth, 21 and mixer IF bandwidth, 21 can additionally prevent the full utilization of the TWPAs multi-GHz bandwidth.

Here, we demonstrate a resonant Josephson parametric amplifier that achieves the bandwidth performance of a matched JPA and a hundred-fold increase in saturation power. The amplifier design is based on the impedance matched parametric amplifier (IMPA), which is in widespread use in our lab for frequency multiplexed readout. Unlike the IMPA, and indeed most JPA implementations, in which the amplifier's nonlinear inductance is provided by a single dc-SQUID (with critical currents of order of a few μ A), the amplifiers presented in this Letter use arrays of high critical current rf-SQUIDs. The substitution of an rf-SQUID array for each of the junctions in the JPA SQUID increases the saturation power of the amplifier while keeping the total inductance of the device roughly the same.

Figure 1(a) shows a simplified diagram of the amplifier. The nonlinear inductance is composed of two rf-SQUID arrays arranged in parallel to form a compound SQUID¹³ with a total of 2N = 40 unit

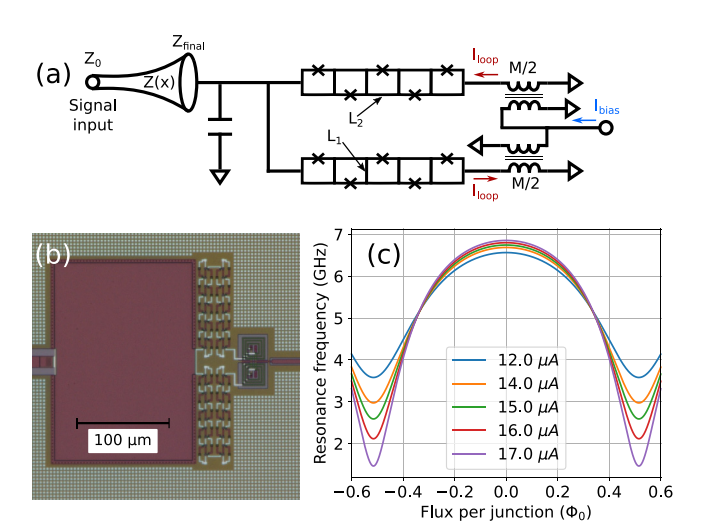


FIG. 1. (a) Circuit diagram of the amplifier. The active element of the circuit consists of a tunable inductor made up of two rf-SQUID arrays in parallel ("snake"). Each rf-SQUID consists of a Josephson junction and geometric inductances L_1 and L_2 , and each array contains 20 rf-SQUIDs. A differential bias coil allows both DC and RF modulation of the inductance, while a shunt capacitor sets the frequency range. A tapered impedance transformer lowers the loaded Q of the device, increasing its bandwidth. (b) Optical micrograph of the nonlinear resonator showing the shunt capacitor, snake inductor, and the bias transformer. (c) Calculated resonance frequency vs applied flux bias per junction (or per rf-SQUID) with 2N=40 rf-SQUID stages, $C_8=6.0$ pF, $L_1=2.6$ pH, $L_2=8.0$ pH, $L_b=30$ pH, and a range of junction I_c .

cells. Each rf-SQUID consists of a junction with critical current I_c , and linear inductance composed of two segments with inductance L_1 and one segment with inductance L_2 . The L_1 segments are shared between neighboring rf-SQUIDs, so that the structure as a whole forms a serpentine inductive spine of alternating L_1 and L_2 , bridged by Josephson junctions at each meander. We will refer to this structure as the "snake," and to the amplifier as a whole as "snake-IMPA" or "SNIMPA" for short. The parallel arrangement of the arrays enables us to flux-bias and pump the amplifier via a single superconducting split-coil spiral transformer as shown in the figure. The transformer primary coils are connected in parallel paths between the bias feedline and ground. The secondary coils are counter-wound to primarily couple the bias to the circulating current mode (I_{loop} in the figure) of the compound SQUID loop formed by the two parallel portions of the snake (see the supplementary material). The transformer mutual inductance is $M \approx 50$ pH, and the self-inductance of the secondary coil is \approx 120 pH. Finally, the structure is shunted by a capacitor C_s and is connected to the $50\,\Omega$ signal port via a Klopfenstein taper as in Ref. 8. An optical micrograph of the shunt capacitor, compound snake-SQUID, and bias transformer is shown in Fig. 1(b).

The resonance frequency of the nonlinear circuit created by the capacitively shunted snake is $\omega_{\text{res}} = 1/\sqrt{(L_s + L_b)C_s}$, where L_s is given by^{13,22} (see the supplementary material)

$$L_s = \frac{N}{2} \times \frac{L_J(L_1 + L_2) + L_1 L_2 \cos \delta_0}{L_J + (4L_1 + L_2) \cos \delta_0},$$
 (1)

 $L_J=\hbar/2eI_c$, and δ_0 is the equilibrium junction phase, which is dependent on the flux bias. ^{13,22} L_b is a stray inductance that includes a contribution from the bias transformer self-inductance. The calculated resonance frequency for typical circuit parameters is shown in Fig. 1(c) as a function of the applied flux bias per junction (or per rf-SQUID) in the array.

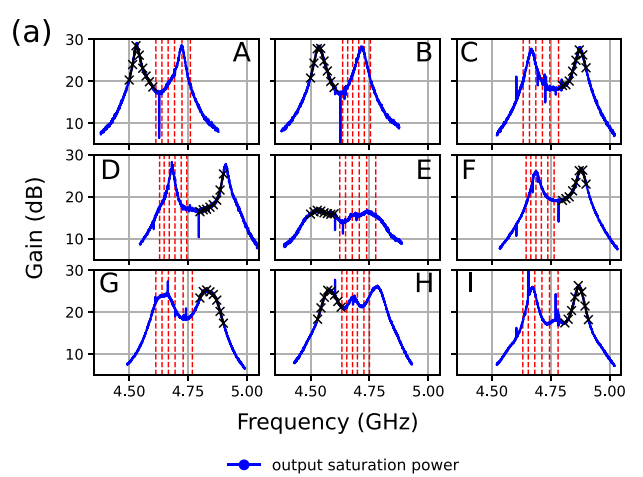
To avoid hysteresis in the modulation curve, the snake must be designed such that $L_J > 4L_1 + L_2$. This means that, unlike a conventional dc-SQUID, the inductance of a snake-SQUID does not diverge at $\Phi_0/2$. Therefore, $\omega_{\rm res}$ has a limited tunability range compared to conventional JPAs, as seen in Fig. 1(c). We, therefore, choose the shunt capacitance C_s such that the frequency tunability range overlaps the desired operating frequency of the amplifier, 4.5–5.0 GHz. The device is flux-pumped at frequency ω_P , which is twice the center frequency of the amplifier.

Here, we report on amplifiers having two design variants. The first, design 1, has a nominal junction $I_c = 16 \,\mu\text{A}$ and a shunt capacitance of $C_s = 6.5$ pF, and the second, design 2, has a nominal $I_c = 18 \,\mu\text{A}$ and $C_s = 6.0 \text{ pF}$. Both designs have nominal snake inductances of $L_1 = 2.6$ pH and $L_2 = 8.0$ pH. From measurement of test junctions, we estimate that the actual critical current of the snake junctions is ≈20% lower than designed. The Klopfenstein taper that matches the low impedance SNIMPA resonator to the 50Ω signal port is similar to that reported in Ref. 8 with a cutoff frequency of 2.6 GHz and a 50-section taper from 51Ω to 24Ω , resulting in a resonator loaded Q of about 4.5. The devices were built in a three-layer aluminum process with SiOx interlayer dielectrics and Al/AlOx/Al trilayer Josephson junctions. The first metal layer was used as a solid ground plane under the snake structure, and the upper two layers form the circuit elements of the amplifier (see the supplementary material). In operation, the amplifiers' dc flux bias amounts to approximately

 $320\,\mu\text{A}$ carried in each of the bias transformer primary coils, well below the measured critical current of traces and vias in our process.

We have characterized the performance of the SNIMPA devices with a 54-qubit Sycamore processor. The processor consists of nine independent readout lines, each with six frequency-multiplexed readout resonators occupying a 4.6–4.8 GHz band. Each readout line has an on-chip Purcell filter and is connected to a SNIMPA amplifier through four circulators. The readout resonators and Purcell filters were designed with a target resonator ringdown time of $1/\kappa = 25$ ns. The readout lines are labeled A–I; lines A, C, E, and G had a SNIMPA with design 1, and the rest had design 2. All SNIMPA were packaged with a magnetic shield. In a separate cooldown, all readout lines were outfitted with standard dc-SQUID based IMPA, whose performance we use as a baseline for comparison.

Figure 2(a) shows the SNIMPA gain vs signal frequency (blue lines) on all readout lines as labeled. Each curve was measured at low power with a vector network analyzer, after manual tuneup of the



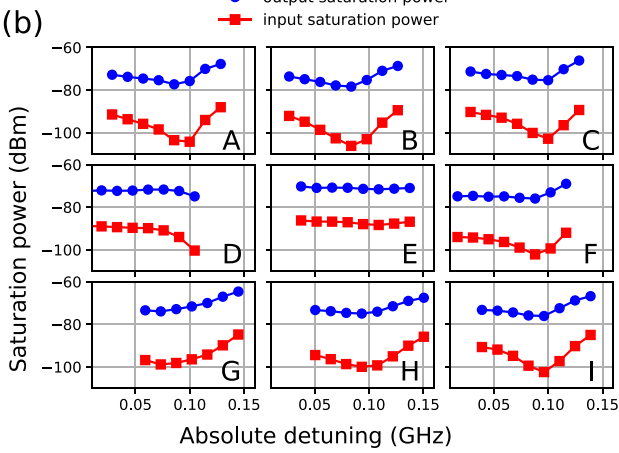


FIG. 2. (a) Gain vs frequency (solid blue lines) of SNIMPA amplifiers for each readout line as labeled. Lines A, C, E, and G use design 1, and the rest use design 2. Vertical lines (dashed red) indicate the frequencies of the readout resonators. Black crosses denote the frequencies at which saturation power was measured. (b) Corresponding input and output saturation power (1-dB gain compression) calibrated at the processor reference plane vs absolute detuning from the amplifier center frequency.

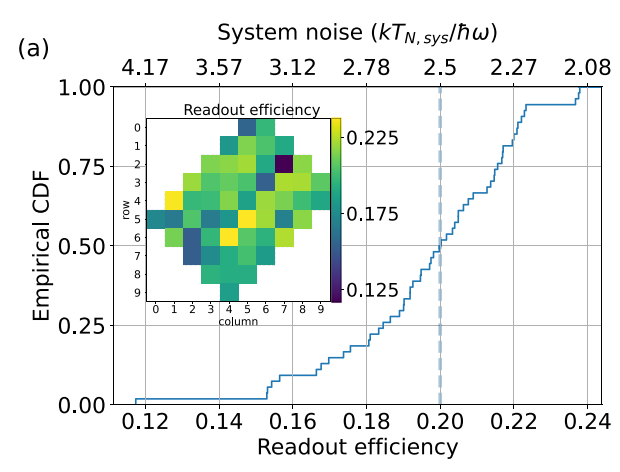
amplifier's flux bias, pump frequency, and pump power. The frequencies of the readout resonators associated with each line are indicated by the vertical dashed lines (red). All amplifiers achieve gains greater than 15 dB over the entire readout band, and most resonators can be readout with a gain exceeding 20 dB. The gain profile is not Lorentzian; this is because the complex impedance seen by the SNIMPA nonlinear resonator varies over the amplifier band. The multi-peak response is commonly seen in wider band parametric amplifiers, \$,23,24 but impedance matching network synthesis techniques could be used to achieve better control of gain flatness and ripple.

For the purpose of the present experiments, we were focused on isolated qubit readout performance. In some cases, we allowed the center frequency of the amplifier to reside within the resonator band (e.g., line H). In simultaneous multi-qubit readout with degenerate parametric amplifiers, in which the signal (at frequency ω_s) and idler (at $\omega_i = \omega_P - \omega_s$) share the same physical circuit, this can cause interference between a signal from one of the resonators and an idler generated by the readout of another. Therefore, in simultaneous multi-qubit readout, the pump should be tuned such that all readout resonator frequencies reside either below or above $\omega_P/2$, meaning that only half the bandwidth is usefully available in practice.

Figure 2(b) shows the input (squares) and output (circles) saturation power (1-dB gain compression) of each of the amplifiers as a function of the absolute signal detuning from the amplifier center frequency (half the pump frequency, $\omega_P/4\pi$). The crosses in Fig. 2(a) denote the frequency and gain at which each point was measured. For this experiment, we calibrate the signal power at the processor reference plane using ac Stark shift of the processor qubits. We first measure the dispersive shift $\chi = (\omega_{r,|0\rangle} - \omega_{r,|1\rangle})/2$ (where $\omega_{r,|0\rangle}$ and $\omega_{r,|1\rangle}$ are the dressed resonance frequencies) and the resonator decay rate κ spectroscopically for each qubit in our processor. From the ac Stark shift, which is given (in the linear regime) by $\delta\omega_{01} = -2\chi\bar{n}$, we extract \bar{n} , the average resonator photon occupation for a given combination of resonator drive power and frequency.²⁵ From the measured values of κ and \bar{n} we calculate the microwave power impinging on the resonator.²⁶ Repeating this measurement at varying powers from the room-temperature signal generator allows us to calibrate the power delivered to the chip as a function of the signal generator power. Figure 2(b) shows that the SNIMPA consistently achieve output saturation powers in the -80 to -70 dBm range, up to 20 dB higher than our standard dc-SQUID based IMPA. While output saturation power, being ideally gain-independent, is the more fundamental quantity, the figure also reports the input saturation power to allow a more direct comparison with the bulk of the existing literature.

We do not measure the amplifier added noise directly. Instead, we focus on the overall readout efficiency, 27 η , which is a more relevant metric from a systems performance perspective (see the supplementary material). Readout efficiency encapsulates all microwave losses, α , between the readout resonators and the SNIMPA, as well as the noise temperature of the SNIMPA itself, T_p , and the effective noise temperature, T_h , of the cryogenic HEMT amplifier and the rest of the measurement chain following the SNIMPA. Since our amplifiers are operated in a phase preserving mode, the maximum possible efficiency is $\eta=0.5$.

Figure 3(a) shows the measured readout efficiency for all qubits in our Sycamore processor. The empirical cumulative distribution function of these data is shown in the main plot with a median of $\eta=0.2$



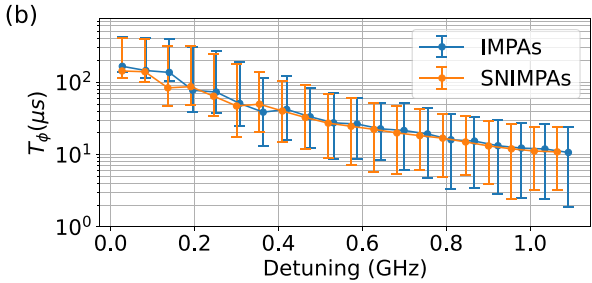


FIG. 3. (a) Cumulative distribution of readout efficiency over 54 qubits, showing a mean (dash-dot line) and median (dashed line) around 20%. The top x-axis represents the equivalent total system noise, expressed in terms of photon number units. Inset: heat-map of readout efficiency by qubit across the processor. (b) Dephasing times, T_{ϕ} , measured using CPMG, vs qubit detuning away from their flux-insensitive, maximum frequency points. Data show the median over all qubits in the processor, and error bars represent the 17–83 percentile range. Data measured with SNIMPA (orange) are compared with those measured with our standard IMPA (blue), showing similar performance of the two amplifier types.

corresponding to a system noise temperature of $T_{N,sys} = 560$ mK. The inset shows how these efficiencies are distributed across the qubit grid.

We measure the readout efficiency, η , and signal-to-noise ratio (SNR) gain, $G_{\rm SNR}$, as a function of the SNIMPA power gain, G_p , for all qubits in our processor

$$G_{\rm SNR} = \frac{G_p(T_Q + T_h)}{G_p T_Q + (G_p - 1)T_p + T_h},$$
 (2)

$$\eta = \frac{\alpha G_p T_Q}{G_p T_Q + (G_p - 1)T_p + T_h},$$
(3)

where $T_Q=\hbar\omega/2k$ is the quantum noise at the readout frequency, and fit the data with both equations simultaneously. Since these fits cannot separate out contributions from α and T_p , we have to fix one of these parameters. If the SNIMPA were quantum limited and we fix $T_p=T_Q$, then fits to our data suggest an average insertion loss of $\alpha=0.44\pm0.03$ or -3.57 dB between the processor chip and the SNIMPA.

Independent, cryogenically calibrated ²⁸ measurements of individual component losses (circulators and wiring) add up to a minimum of $-2.5\,\mathrm{dB}$ of loss between the processor chip and the SNIMPA (see

the supplementary material). If we, therefore, fix $\alpha=0.56$ (-2.5 dB) in the fits, then we can extract a maximum SNIMPA noise temperature, $T_p=0.18\pm0.02$ K, roughly 60% higher than the quantum limit. A cryogenically calibrated measurement of a representative integrated readout assembly shows an insertion loss that varies between -3.6 and -2.7 dB over the readout band (see the supplementary material). These data put bounds on the average noise performance of the SNIMPA, as deployed, in the context of qubit readout of our processor. The data suggest that after accounting for component losses, the measured efficiencies are consistent with near quantum limited noise performance of the SNIMPA amplifiers.

A potential concern with the SNIMPA is that the snake inductor could increase back action on the qubit, compared to the standard dc-SQUID based amplifiers. This could be due to coupling of noise photons through the large bias transformer, pump leakage to the signal line, or the generation of spurious signals or noise during amplification. Figure 3(b) shows qubit dephasing time, T_{ϕ} , as measured using the CPMG (Carr-Purcell-Meiboom-Gill) method²⁹ vs qubit detuning away from their flux-insensitive point. The data, representing the median over all qubits in the processor, compare the performance measured with the SNIMPAs (orange) to that measured in a separate cooldown of the same processor with the standard IMPA amplifiers (blue). The data indicate that the SNIMPAs have no adverse effect on qubit dephasing as compared to our standard dc-SQUID based amplifiers.

Finally, we performed multi-tone experiments to test the SNIMPA performance in an emulated simultaneous multi-qubit readout scenario. We chose to do so, instead of directly characterizing multi-qubit readout fidelity, to avoid confounding qubit-related physics at high readout powers² that can mask the underlying performance of the amplifiers. As a baseline, we first measure the amplifier signal power gain and SNR improvement (SNR gain) as a function of frequency with a single ("isolated"), weak readout tone (approximately $-130 \,\mathrm{dBm}$), as shown in Fig. 4(a). We then repeat the measurement with five additional tones (emulating the six-qubit multiplexed readout in the Sycamore processor) and with each tone having 10 dB higher power, as illustrated in Fig. 4(b). Here, each one of the readout tones is swept in turn across its corresponding frequency band (respective color), and we measure the signal and SNR gains while the others tones are on and are kept at the fixed frequencies indicated by the respective vertical dashed lines. Figures 4(c) and 4(d) show the gain and SNR improvement, respectively, for our standard dc-SQUID based IMPA, clearly showing degradation in both quantities in the multi-tone experiment (color) compared with the low-power baseline (black). In contrast, no such degradation is observed with the SNIMPA, as shown in Figs. 4(e) and 4(f). In fact, we found it difficult to drive the SNIMPA to saturation with our standard readout electronics setup. These experiments demonstrate that the SNIMPA's high saturation power offers sufficient headroom in a multi-qubit readout situation to enable more efficient readout multiplexing with higher number of qubits read-out simultaneously per channel. The SNIMPA can also accommodate higher power per readout tone, which may be required for high-fidelity, fast readout with greater qubit-resonator detuning or weaker qubit-resonator coupling.

In summary, we have demonstrated impedance matched Josephson parametric amplifiers with saturation powers up to two orders of magnitude higher than their standard dc-SQUID based

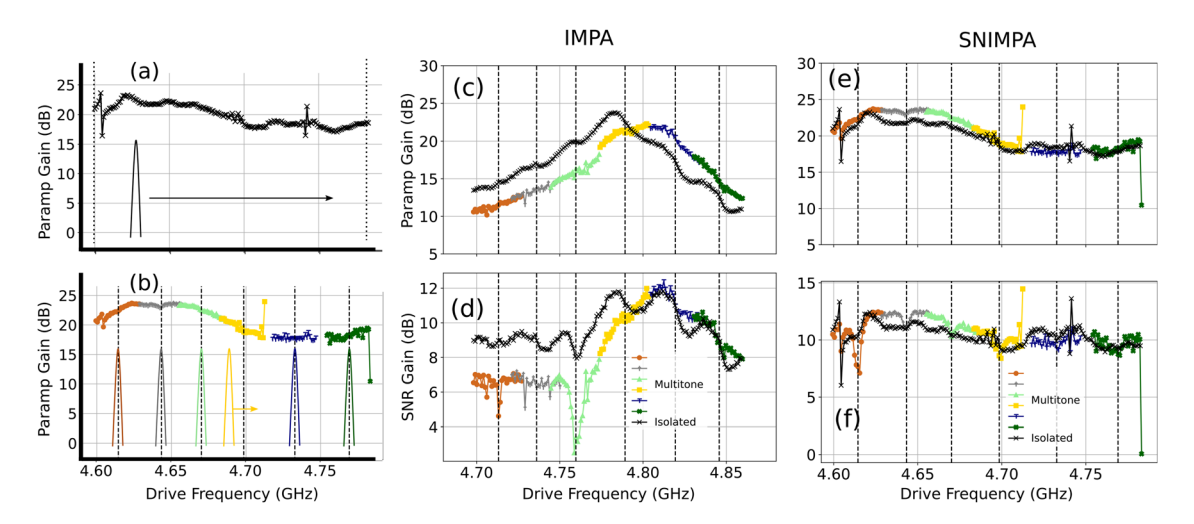


FIG. 4. Multi-tone readout experiments. (a) and (b) Description of the experiment. (a) The amplifier gain is measured with a single tone at low power levels, typically —130 dBm, and the single tone is swept across the full readout band, and (b) gain is measured for each one of six readout tones as it is swept in turn across its corresponding frequency band (colored sections) while the other five tones are held at fixed frequencies as indicated by the respective vertical dashed lines. In this experiment, each of the six tones are roughly —120 dBm, i.e., 10 dB higher power per tone than the baseline. (c) Measured power gain and (d) SNR gain in the multi-tone experiment (color, "multitone") compared to baseline (black, "isolated") for a traditional IMPA amplifier. The IMPA shows a shift in the gain profile and a degradation of the SNR gain due to saturation. (e) and (f) Results of the same experiment using the SNIMPA amplifier on readout line G, which shows little change in power gain and SNR gain when driven simultaneously with six high power tones, as compared to the single tone low power baseline.

counterparts. By combining an rf-SQUID array nonlinear element with an impedance matching taper, these amplifiers achieve sufficient instantaneous bandwidth to support 6:1 frequency-multiplexed readout of our Sycamore processors. We have measured a median readout efficiency of 20%, extracted an upper bound for the SNIMPA noise temperature at around 60% over the quantum limit, and found no excess amplifier-related dephasing compared to our standard IMPA-based setup.

See the supplementary material for details on the derivation of the snake inductance, transformer design, efficiency measurement, and loss budget estimates.

AUTHOR DECLARATIONS Conflict of Interest

The authors have no conflicts to disclose.

Author Contributions

Theodore White: Conceptualization (equal); Data curation (equal); Formal analysis (equal); Investigation (equal); Methodology (equal); Software (equal); Visualization (lead); Writing - original draft (lead); Writing - review & editing (equal). Joseph C. Bardin: Investigation (supporting). Andreas Bengtsson: Software (supporting). Alexandre Bourassa: Software (supporting). Jenna Bovaird: Investigation (supporting). Leon Brill: Resources (supporting). Bob Buckley: Investigation (supporting). David Buell: Project administration (supporting); Resources (supporting). Tim Burger: Investigation (supporting). Brian Burkett: Investigation (supporting); Supervision (supporting). Nicholas Investigation (supporting). Alexander Opremcak: Investigation (equal); Methodology (equal); Software (equal). Zijun Chen: Software (supporting). Ben Chiaro: Investigation (supporting); Software (supporting). Josh Cogan: Software (supporting). Roberto Collins: Investigation (supporting). Alexander L. Crook: Investigation (supporting). Ben Curtin: Investigation (supporting). Sean Demura: Investigation (supporting). Andrew Dunsworth: Investigation (supporting); Software (supporting). Catherine Erickson: Investigation (supporting); Resources (supporting); Software (supporting). Reza Fatemi: Investigation (supporting). George Sterling: Investigation (equal); Software (equal). Leslie Flores: Investigation (supporting). Ebrahim Forati: Investigation (supporting). Brooks Foxen: Investigation (supporting). William Giang: Investigation (supporting). Marissa Giustina: Investigation (supporting); Software (supporting). Alejandro Garjales Dau: Investigation (supporting). Michael C. Hamilton: Investigation (supporting). Sean D. Harrington: Investigation (supporting). Jeremy Hilton: Investigation (supporting). Markus Hoffmann: Project administration (supporting). Alexander Korotkov: Formal analysis (equal); Methodology (equal). Sabrina Hong: Software (supporting). Trent Huang: Investigation (supporting). Ashlev Huff: Resources (supporting). Justin Iveland: Investigation (supporting). Evan Jeffrey: Investigation (supporting); Software (supporting). Marika Kieferova: Software (supporting). Seon Kim: Investigation (supporting). Paul V. Klimov: Investigation (supporting); Software (supporting). Fedor Kostritsa: Software (supporting). John Mark Kreikebaum: Investigation (supporting). Daniel Sank: Formal analysis (equal); Methodology (equal). David Landhuis: Investigation (supporting); Resources (supporting). Pavel Laptev: Investigation (supporting); Resources (supporting). Lily Laws: Funding acquisition (supporting); Project administration (supporting); Resources (supporting). Kenny Lee: Software (supporting). Brian J. Lester: Software (supporting). Alexander Lill: Investigation (supporting). Wayne Liu: Investigation (supporting). Aditya Locharla: Software (supporting). Erik Lucero: Funding acquisition (supporting); Project administration

(supporting); Resources (supporting); Supervision (supporting). Trevor McCourt: Software (supporting). Rajeev Acharya: Investigation (supporting). Matt McEwen: Software (supporting). Xiao Mi: Software (supporting). Kevin C Miao: Software (supporting). Shirin Montazeri: Investigation (supporting). Alexis Morvan: Software (supporting). Matthew Neeley: Software (supporting). Charles Neill: Software (supporting). Ani Nersisyan: Software (supporting). Jiun How Ng: Investigation (supporting). Anthony Nguyen: Investigation (supporting). Markus Ansmann: Software (supporting). Murray Nguyen: Investigation (supporting). Rebecca Potter: Project administration (supporting). Chris Quintana: Software (supporting). Pedram Roushan: Software (supporting). Kannan Sankaragomathi: Investigation (supporting). Kevin Joseph Satzinger: Software (supporting). Christopher Schuster: Project administration (supporting). Michael J. Shearn: Investigation (supporting); Resources (supporting). Aaron Shorter: Investigation (supporting). Vladimir Shvarts: Resources (supporting). Frank Arute: Investigation (supporting). Jindra Skruzny: Resources (supporting). W. Clarke Smith: Investigation (supporting). Marco Szalay: Investigation (supporting); Resources (supporting); Software (supporting). Alfredo Torres: Investigation (supporting). Bryan Woo: Investigation (supporting). Z. Jamie Yao: Investigation (supporting). Ping Yeh: Software (supporting). Juhwan Yoo: Investigation (supporting). Grayson Young: Resources (supporting). Ningfeng Zhu: Investigation (supporting). Kunal Arya: Software (supporting). Nicholas Zobrist: Investigation (supporting); Software (supporting). Yu Chen: Project administration (supporting); Supervision (supporting). Anthony Megrant: Investigation (supporting); Project administration (supporting); Supervision (equal). Julian Kelly: Investigation (supporting); Project administration (supporting); Software (supporting); Supervision (equal). Ofer Naaman: Conceptualization (lead); Formal analysis (equal); Investigation (equal); Methodology (equal); Software (equal); Supervision (equal); Validation (equal); Visualization (equal); Writing original draft (lead); Writing - review & editing (equal).

DATA AVAILABILITY

The data that support the findings of this study are available from the corresponding authors upon reasonable request.

REFERENCES

- ¹A. Wallraff, D. Schuster, A. Blais, L. Frunzio, J. Majer, M. Devoret, S. Girvin, and R. Schoelkopf, "Approaching unit visibility for control of a superconducting qubit with dispersive readout," Phys. Rev. Lett. **95**, 060501 (2005).
- ²D. Sank, Z. Chen, M. Khezri, J. Kelly, R. Barends, B. Campbell, Y. Chen, B. Chiaro, A. Dunsworth, A. Fowler *et al.*, "Measurement-induced state transitions in a superconducting qubit: Beyond the rotating wave approximation," Phys. Re. Let. 117, 190503 (2016).
- ³R. Vijay, D. Slichter, and I. Siddiqi, "Observation of quantum jumps in a superconducting artificial atom," Phys. Rev. Lett. 106, 110502 (2011).
- ⁴N. Roch, E. Flurin, F. Nguyen, P. Morfin, P. Campagne-Ibarcq, M. H. Devoret, and B. Huard, "Widely tunable, nondegenerate three-wave mixing microwave device operating near the quantum limit," Phys. Rev. Lett. **108**, 147701 (2012).
- J. Mutus, T. White, E. Jeffrey, D. Sank, R. Barends, J. Bochmann, Y. Chen, Z. Chen, B. Chiaro, A. Dunsworth *et al.*, "Design and characterization of a lumped element single-ended superconducting microwave parametric amplifier with on-chip flux bias line," Appl. Phys. Lett. **103**, 122602 (2013).

- ⁶J. Aumentado, "Superconducting parametric amplifiers: The state of the art in Josephson parametric amplifiers," IEEE Microwave Mag. **21**, 45–59 (2020).
- 7F. Arute, K. Arya, R. Babbush, D. Bacon, J. C. Bardin, R. Barends, R. Biswas, S. Boixo, F. G. Brandao, D. A. Buell *et al.*, "Quantum supremacy using a programmable superconducting processor," Nature 574, 505–510 (2019).
- ⁸J. Mutus, T. White, R. Barends, Y. Chen, Z. Chen, B. Chiaro, A. Dunsworth, E. Jeffrey, J. Kelly *et al.*, "Strong environmental coupling in a Josephson parametric amplifier," Appl. Phys. Lett. **104**, 263513 (2014).
- ⁹T. Roy, S. Kundu, M. Chand, A. Vadiraj, A. Ranadive, N. Nehra, M. P. Patankar, J. Aumentado, A. Clerk, and R. Vijay, "Broadband parametric amplification with impedance engineering: Beyond the gain-bandwidth product," Appl. Phys. Lett. 107, 262601 (2015).
- 10 P. Duan, Z. Jia, C. Zhang, L. Du, H. Tao, X. Yang, L. Guo, Y. Chen, H. Zhang, Z. Peng et al., "Broadband flux-pumped Josephson parametric amplifier with an on-chip coplanar waveguide impedance transformer," Appl. Phys. Express 14, 042011 (2021).
- ¹¹O. Naaman and J. Aumentado, "Synthesis of parametrically coupled networks," PRX Quantum 3, 020201 (2022).
- ¹²N. Frattini, V. Sivak, A. Lingenfelter, S. Shankar, and M. Devoret, "Optimizing the nonlinearity and dissipation of a SNAIL parametric amplifier for dynamic range," Phys. Rev. Appl. 10, 054020 (2018).
- ¹³O. Naaman, D. G. Ferguson, A. Marakov, M. Khalil, W. F. Koehl, and R. J. Epstein, "High saturation power Josephson parametric amplifier with GHz bandwidth," in 2019 IEEE MTT-S International Microwave Symposium (IMS) (IEEE, 2019), pp. 259–262.
- ¹⁴C. Macklin, K. O'brien, D. Hover, M. Schwartz, V. Bolkhovsky, X. Zhang, W. Oliver, and I. Siddiqi, "A near-quantum-limited Josephson traveling-wave parametric amplifier," Science 350, 307–310 (2015).
- ¹⁵K. O'Brien, C. Macklin, I. Siddiqi, and X. Zhang, "Resonant phase matching of Josephson junction traveling wave parametric amplifiers," Phys. Rev. Lett. 113, 157001 (2014).
- ¹⁶C. Bockstiegel, J. Gao, M. Vissers, M. Sandberg, S. Chaudhuri, A. Sanders, L. Vale, K. Irwin, and D. Pappas, "Development of a broadband NbTiN traveling wave parametric amplifier for MKID readout," J. Low. Temp. Phys. 176, 476–477 (2014).
- ¹⁷B. H. Eom, P. K. Day, H. G. LeDuc, and J. Zmuidzinas, "A wideband, low-noise superconducting amplifier with high dynamic range," Nat. Phys. 8, 623–627 (2012).
- ¹⁸M. Esposito, A. Ranadive, L. Planat, and N. Roch, "Perspective on traveling wave microwave parametric amplifiers," Appl. Phys. Lett. 119, 120501 (2021).
- ¹⁹K. Peng, M. Naghiloo, J. Wang, G. D. Cunningham, Y. Ye, and K. P. O'Brien, "Floquet-mode traveling-wave parametric amplifiers," PRX Quantum 3, 020306 (2022).
- ²⁰R. Barends, J. Kelly, A. Megrant, A. Veitia, D. Sank, E. Jeffrey, T. White, J. Mutus, A. Fowler, B. Campbell *et al.*, "Superconducting quantum circuits at the surface code threshold for fault tolerance," Nature 508, 500–503 (2014).
- ²¹E. Jeffrey, D. Sank, J. Mutus, T. White, J. Kelly, R. Barends, Y. Chen, Z. Chen, B. Chiaro, A. Dunsworth *et al.*, "Fast accurate state measurement with superconducting qubits," Phys. Rev. Lett. 112, 190504 (2014).
- 22O. Naaman, J. Strong, D. Ferguson, J. Egan, N. Bailey, and R. Hinkey, "Josephson junction microwave modulators for qubit control," J. Appl. Phys. 121, 073904 (2017).
- ²³J. Grebel, A. Bienfait, É. Dumur, H.-S. Chang, M.-H. Chou, C. Conner, G. Peairs, R. Povey, Y. Zhong, and A. Cleland, "Flux-pumped impedance-engineered broadband Josephson parametric amplifier," Appl. Phys. Lett. 118, 142601 (2021).
- ²⁴L. Ranzani, G. Ribeill, B. Hassick, and K. C. Fong, "Wideband Josephson parametric amplifier with integrated transmission line transformer," preprint arXiv:2208.02331 (2022).
- ²⁵D. I. Schuster, A. A. Houck, J. A. Schreier, A. Wallraff, J. M. Gambetta, A. Blais, L. Frunzio, J. Majer, B. Johnson, M. H. Devoret, S. M. Girvin, and R. J. Schoelkopf, "Resolving photon number states in a superconducting circuit," Nature 445, 515–518 (2007).
- ²⁶R. Vijay, C. Macklin, D. Slichter, S. Weber, K. Murch, R. Naik, A. N. Korotkov, and I. Siddiqi, "Stabilizing Rabi oscillations in a superconducting qubit using quantum feedback," Nature 490, 77–80 (2012).

- ²⁷C. C. Bultink, B. Tarasinski, N. Haandbæk, S. Poletto, N. Haider, D. Michalak, A. Bruno, and L. DiCarlo, "General method for extracting the quantum efficiency of dispersive qubit readout in circuit QED," Appl. Phys. Lett. 112, 092601 (2018).
- ²⁸H. Wang, S. Singh, C. McRae, J. Bardin, S. Lin, N. Messaoudi, A. Castelli, Y. Rosen, E. Holland, D. Pappas *et al.*, "Cryogenic single-port calibration for
- superconducting microwave resonator measurements," Quantum Sci. Technol. **6**, 035015 (2021).
- ²⁹J. Bylander, S. Gustavsson, F. Yan, F. Yoshihara, K. Harrabi, G. Fitch, D. G. Cory, Y. Nakamura, J.-S. Tsai, and W. D. Oliver, "Noise spectroscopy through dynamical decoupling with a superconducting flux qubit," Nat. Phys. 7, 565–570 (2011).